




Effect of post-weld heat treatment on the microstructure and tensile properties of electron-beam-welded 21st century nickel-based super alloy 686

B ARULMURUGAN^{1,3,*}, KUNJAN MODI¹, AMRUTKAR PRANIT SANJAY¹,
PATIL APURVA YASHWANT¹, N RICKWITH¹, C G MOHAN¹, P SUBRAMANI¹, M AGILAN²,
M MANIKANDAN^{1,*}  and N ARIVAZHAGAN¹

¹School of Mechanical Engineering, Vellore Institute of Technology, Vellore, India

²Materials Processing Research Group, Vikram Sarabhai Space Center, ISRO, Trivandrum, India

³KPR Institute of Engineering and Technology, Coimbatore, India

e-mail: enggarul@gmail.com; mano.manikandan@gmail.com

MS received 27 June 2018; revised 1 November 2018; accepted 14 November 2018

Abstract. This work examines the influence of post-weld heat treatment (PWHT) on the fusion zone microstructure, and mechanical properties of electron beam (EB)-welded alloy 686. Comparative studies have been made on weld microstructure and tensile properties of the weldments both in as-welded and post-welded heat-treated conditions. PWHT consists of direct aging (DA/480°C for 3 h) and solution treatment (ST, 980°C for 1 h) followed by ageing and finally, homogenizing treatment (HT, 1200°C for 1 h) followed by DA and ST. The secondary topologically closed packed (TCP) phases formation, their distribution and microsegregation characteristics are studied with the aid of scanning electron microscope (SEM) analysis. Energy-dispersive X-ray spectroscopy (EDS) is also performed to estimate the microsegregation of alloying elements in the dendritic core and interdendritic regions of the weldments. The result shows that there is no significant change in the microstructure of DA and solution-treated sample as compared to the as-welded sample. The microstructure of HT sample was entirely different from those of as-welded and other HT samples. The SEM/EDS analysis illustrates the presence of secondary TCP phases (σ , P and μ) in the as-weld, DA and ST condition, whereas HT weldments did not show the presence of TCP phases. Tensile test results show higher tensile strength in ST condition whereas homogenization samples show higher ductility compared with others.

Keywords. Alloy 686; electron beam welding; post-weld heat treatment; direct aging; solution treating; homogenization.

1. Introduction

Alloy 686 (UNS N06686) is a high-corrosion-resistance nickel-based superalloy developed in the year 1992. This alloy resulted from a Ni–Cr–Mo ternary system [1]. The alloy was developed from the alloys C-276 and C-22 with minor modification in its chemical composition [2]. The presence of chromium (Cr) in the alloy provides resistance against oxidation environment. Molybdenum (Mo) works effectively in reducing environments and it is prone to pitting and crevice corrosion. Tungsten (W) content in alloy 686 is noted to be favourable in resisting microfissuring of the weld metal. It also forms a passive layer to provide resistance against pitting corrosion [3]. The low presence of carbon (0.01%) helps in mitigation of grain boundary precipitation. Further, reducing the iron content in this highly

alloyed material from 5% to 1% permits the addition of more nickel, which significantly increases the stability of the matrix. Iron also offers resistance to intergranular attack (IGA) along with titanium content at elevated temperature [4].

Due to exceptional resistance to corrosion in a broad range of environment, alloy 686 is widely used in chemical processing, marine environment and air pollution control (flue gas desulphurization) industries [5]. The structure of intermetallic TCP phases (P, μ and σ) leads to hot cracking in the weldments and causes premature failure during their service. The segregation of alloying elements Mo and Cr is primarily responsible for the observed TCP phases. Many single-phase Ni–Cr–Mo alloys (C-276, C22, 625 and 686) exhibit compositions that are beyond the solubility limit. It gives enough time for the alloys to get exposed at an elevated temperature, which can lead to a wide range of brittle secondary phases.

*For correspondence

In general, face centred cubic (FCC) crystal structure of Ni-based alloys leads to very low diffusion rates of substitutional alloying elements. This, in turn, leads to wide range of microsegregation during solidification. Accordingly, various unanticipated TCP phases (σ , P and μ) form during the solidification. These phases will, in turn, reduce the strength and can promote premature failure [6]. Many researchers reported that the formation of secondary TCP phase would (i) diminish primary alloying elements required for hardening from the matrix, (ii) characterize a weak-zone microstructure between the TCP phase and the matrix interface, (iii) act as a pronounced zone for easy crack initiation and propagation due to its inherent brittle character and (iv) deteriorate the mechanical properties, especially tensile ductility, fracture toughness, fatigue and creep rupture properties [7].

Silva *et al* [8] identified that the intermetallic phase in alloy 686 is a combination of σ , p and μ phases; the authors reported that the formation of these phases is responsible for the weld metal hot cracking in this alloy. During welding, the molten liquid is changed into the FCC phase upon solidification. The secondary phase formed at the final stage of solidification is σ phase, which then becomes P phase by solid state transformation. Finally, the precipitation of the μ phase occurs through the decomposition of the P phase, and the resultant microstructure is formed by liquid- ν - σ -P- μ phase.

The hot cracking tendency can be controlled by appropriate welding process and the proper selection of weld consumables. This can be achieved well using a low heat input and large-cooling-rate welding process such as pulsed current gas tungsten arc welding (PCGTAW) [9].

Arulmurugan and Manikandan [10, 11] investigated the microstructure, microsegregation and mechanical properties of alloy 686 by current pulsing technique. The authors identified that there is a minimization of secondary phase formation during current pulsing, which will reflect in the enhancement of mechanical properties. Also, the authors stated that the formation of secondary phases could be minimized by proper selection of filler wire. Arulmurugan *et al* [12] also studied the electron beam welding (EBW) of alloy 686. The authors noted the formation of secondary phases in the interdendritic zones of the weldment.

In general, post-weld heat treatment (PWHT) must be carried out in the precipitation-strengthened nickel-based superalloy to improve the properties of the weldments [13–15]. Solid-solution-strengthened alloys also require PWHT to minimize the segregation (as a result of solidification in the fusion zone, during welding) in order to maintain the solid solution strengthening effect in the fusion zone. Dissolution of secondary TCP brittle phases is also possible in PWHT, which will result in enhancement of metallurgical and mechanical properties. In addition to this, PWHT was carried out on weldments of solid-solution-strengthened alloys for residual stress

relievement, homogenization, increasing dimensional stability and enhancement of mechanical properties and corrosion behaviour. PWHT provided decremental concentration gradients in fusion zone in order to regain the resistance towards corrosion in weldments [6, 16, 17]. Thus far, there is no literature available on the microsegregation suppression through PWHT on EBW of alloy 686.

Some of the welding techniques incorporated with PWHT in Ni-based alloys to mitigate the severity of secondary phases and improvement in mechanical properties are given here for better understanding.

Madhusudhan Reddy *et al* [18] analysed the effect of different electron beam oscillation techniques to control niobium (Nb) microsegregation and Laves phase formation in Inconel 718. Also, they investigated the effects of PWHTs on mechanical properties of the material. The authors concluded that elliptical oscillation technique leads to less Nb segregation and fine Laves in the interdendritic region. The use of 980°C post-weld solution treatment (ST) produces better tensile ductilities compared with direct aging (DA) treatment without affecting the strength properties.

Cao *et al* [7] investigated the influence of PWHT of laser-welded Inconel 718 alloy on metallurgical characteristics and tensile properties. The authors suggested that the post-weld aging heat treatment can significantly boost the tensile strengths, particularly if welded in the ST condition, when compared with the as-welded condition. Kun Yu *et al* [19] investigated the microstructure and mechanical properties of GH 3535 solid-solution-strengthened nickel-based superalloy using laser welding and also studied the effect of PWHT. The authors identified that there was an increment in both tensile strength and percentage elongation when PWHT was employed.

El-Dasher *et al* [20] analysed the TCP phase dissolution and recrystallization in multi-pass welding of alloy C-22. They observed relatively low mechanical properties in the weldment. They reported that the strength of the weld joints is improved after employing proper solution heat treatments. Edgecumbe Summers *et al* [21] studied the mechanical properties of gas tungsten arc (GTA) welded alloy C-22 in as-welded and heat-treated conditions. The authors identified that the TCP phases offer a slight increase in strength, but TCP also serves as nucleation sites for micro-voids during plastic deformation. This initiates earlier failure during straining. The authors also investigated the influence of aging temperatures and strengthening effect.

Since alloy 686 had developed from alloy C-22, a similar beneficial effect can be expected in alloy 686, in terms of secondary phase dissolution and improvement in mechanical properties of the weld joint. The objective of the present study is to analyse the effect of PWHT on the mechanical property of electron-beam-welded alloy 686.

Table 1. Chemical composition of Inconel 686.

Base/filler metal	Chemical composition (wt%)								
	Ni	Mo	Cr	W	Mn	Fe	S	Co	Others
Inconel alloy 686	Bal.	15.83	19.88	3.215	0.312	0.858	0.17	Nil	0.008 (P), 0.076 (Si), 0.005 (Ti), 0.01 (C)

2. Experimental details

2.1 Material and EBW

A hot-rolled and solution-annealed 3-mm-thick alloy 686 sheet was procured and utilized for this study. The chemical composition of alloy 686 is shown in table 1.

An EBW machine (make: EO PATON) having a capacity of 6 kW power and 60 kV voltage was used to fabricate the weld joints. Using a wire cut electrical discharge machining (EDM) machine, weld coupons were sliced into the dimensions of 3 mm × 55 mm × 160 mm. The process parameters employed in the present study to fabricate the weld joint are listed in table 2. The weld defects were investigated by macro-examination, and no cracks were identified in the weldment.

2.2 Heat treatment

After butt EBW, the weld specimens were subjected to PWHT at three different conditions (i) DA at 480°C/3 h/air cooling, (ii) ST at 980°C/1 h/air cooling + DA at 480°C/3 h/air cooling and (iii) homogenizing treatment (HT) at 1200°C/1 h/ air cooling + ST at 980°C/1 h/air cooling + aging at 480°C/3 h/air cooling.

2.3 Microstructure examination

Standard metallographic procedures were performed to divulge the microstructure. The samples were polished manually with different grades (240–2000) of silicon carbide emery sheets. Then alumina (0.5- μ m grain) and water polishings were carried out using a double disc polishing machine to attain mirror finish. Finally, electrolytic etching was performed on the welded samples to disclose structure-related information. Etching details are given in table 3.

An optical microscope and a scanning electron microscope (SEM) were used to reveal the microstructure of the fusion zone and heat-affected zone (HAZ) of different post-weld-heat-treated weld samples. Energy-dispersive X-ray

Table 2. Welding parameters.

Welding current	Voltage	Welding speed
50 mA	60 kV	25 mm/s

Table 3. Etchants used in electrolytic etching to reveal the microstructure.

PWHT process	Chemical agent	Time duration (s)
Aging-treated sample	Oxalic acid	20–25
Solution-treated sample	Oxalic acid	15–20
Homogenizing-treated sample	Chromic acid	10–15

spectroscopy (EDS) analysis was also carried out to evaluate the microsegregation of alloying elements in the interdendritic region and dendritic core of the weldments.

2.4 Tensile test

In order to evaluate the material's ability to withstand load during its service, a tensile test was carried out on all the samples using a universal testing machine (Instron make 8801). The tensile test coupons were sliced as per ASTM E8/E-8M-13a (sub-size) standard and the test was performed in ambient condition. In each condition, three samples were tested to ensure the reproducibility of the results.

3. Results and discussion

3.1 Microstructure of as-EBW sample

Figures 1(a) and (b) show the microstructure of the as-welded sample. The microstructure shown in figure 1(a) is that of the centre of the fusion zone (CFZ). The fine equiaxed grain structure observed at the CFZ weld centre (figure 1(a)) is due to rapid solidification, which is the outcome of low thermal gradient (G) and high solid–liquid interface velocity (L). This mechanism (low G/L) enhances the formation of new grains and lowers the grain growth. Steep thermal gradient and lower solid–liquid interface velocity (high G/L) ends up with columnar dendritic structure near fusion boundary in TFZ microstructure (figure 1(b)).

Figure 2 shows a higher magnification SEM micrograph of the weld CFZ. SEM analysis reveals the formation of secondary TCP phases and microsegregation of alloying elements in the interdendritic region of the weldment. EDS analysis was performed to quantify the microsegregation of

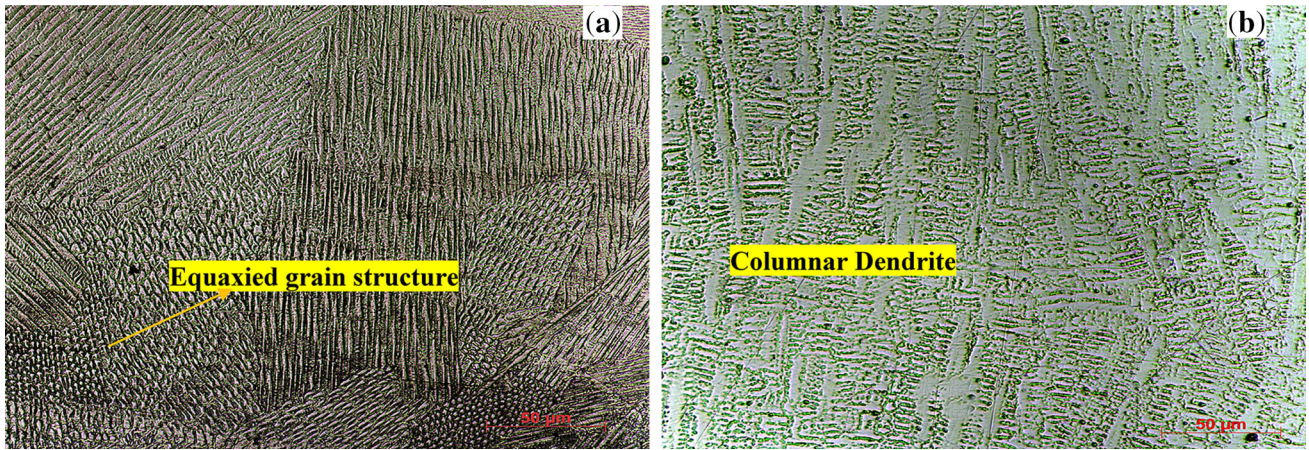


Figure 1. Optical microstructure image of weld joint fabricated by EBW: (a) centre fusion zone and (b) transition fusion zone.

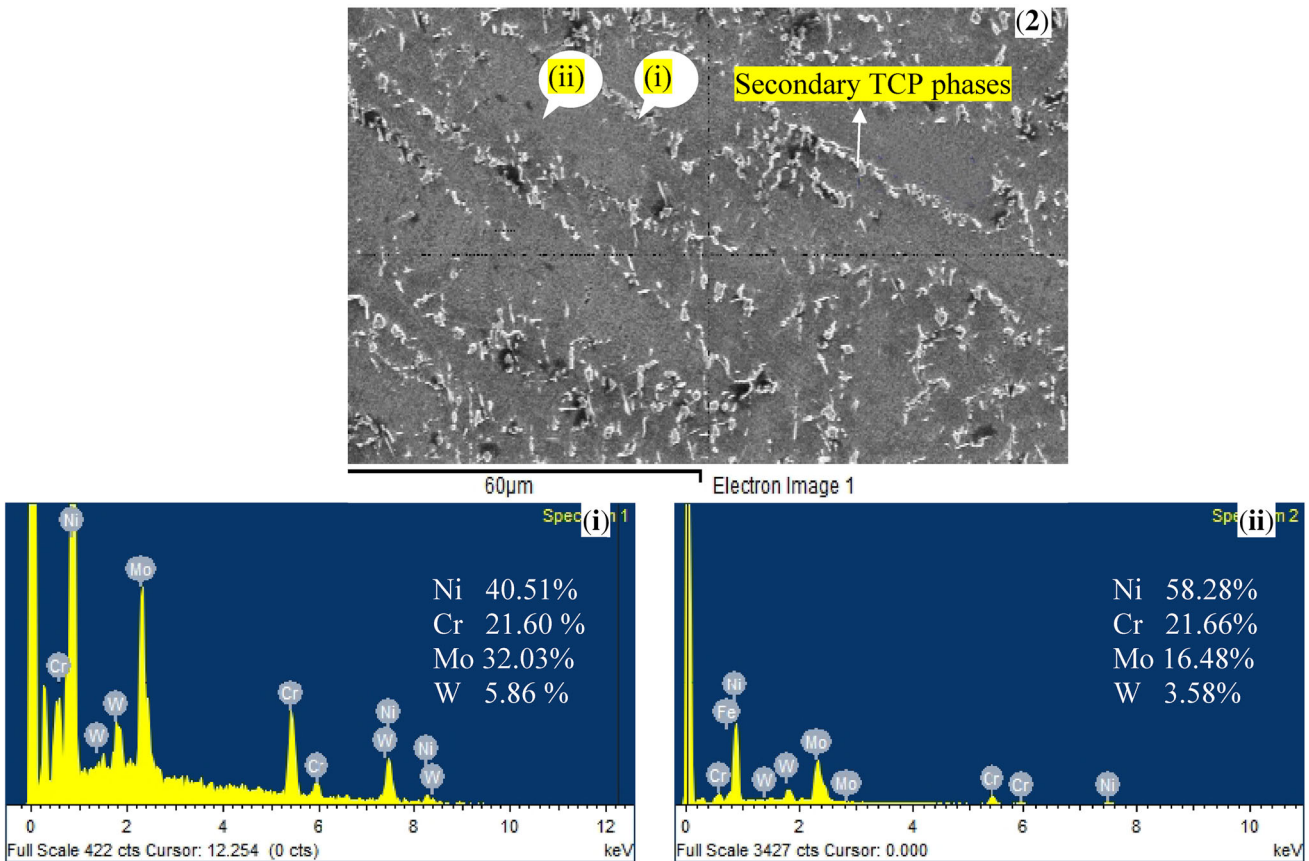


Figure 2. SEM/EDS Analysis of EB Welded alloy 686 (a) SEM image – Weld Centre, (i) EDS analysis of Weld Centre interdendritic region, (ii) EDS analysis of weld centre dendritic core.

alloying elements in the interdendritic region and dendritic core. The presence of secondary TCP phases and microsegregation were recognized by EDS analysis (figure 2 (ii)), which indicates that alloying elements Mo and W are enriched, and depletion of Ni content in the interdendritic region compared with the dendritic core (figure 2

(i)). Despite large cooling rate offered by the EBW process, moderate microsegregation is still observed. This is due to the addition of more alloying elements into the Ni matrix (> 15% Mo) to increase the solid solution strengthening effect; during the eutectic reaction the solubility limit is surpassed, which causes segregation in the interdendritic

regions of the weldments [6]. The main secondary phases in the alloy 686 weldment are identified as σ (tetragonal), P (orthorhombic) and μ (rhombohedral) phases. The P phase occurs in the temperature range of 950–1050°C [22] whereas σ phase is formed in the range of 540–980°C [8] and μ phase evolves in the temperature range of 540–870°C [23]. In the present investigation, the chemical composition of P and μ phases closely matches those reported in the existing literature [8].

3.2 DA-treated microstructure

Figure 3 shows the aging microstructure of the EBW sample. Any perceivable changes in weld microstructure were not noticed after DA treatment. Microstructures in DA condition were similar to those in the as-welded condition. It is observed in the aging microstructure that it contains coarse columnar dendrites. The aging temperature is much lower than secondary TCP phases dissolving temperature. Since aging was carried out at the temperature of 480°C, no significant microstructural change and dissolution of TCP phases were found in the weldment. SEM images (figure 4) confirmed the existence of secondary TCP phases, but their distribution was limited and well separated all over the matrix like discrete particles. As observed, the secondary phase existences are higher in the aging treatment as compared with the as-welded condition. EDS analysis of the weld centre is shown in figures 4 (i) and (ii).

From EDS analysis it is clear that the level of segregation of alloying elements both in interdendritic region and dendritic core is significant. From table 4 it is confirmed that the existence of secondary TCP phases is due to the enrichment of alloying elements like Cr, Mo and W in the interdendritic region. High Cr content leads to the formation of σ phases. Similarly, high Mo content promotes the formation of P phases [6].

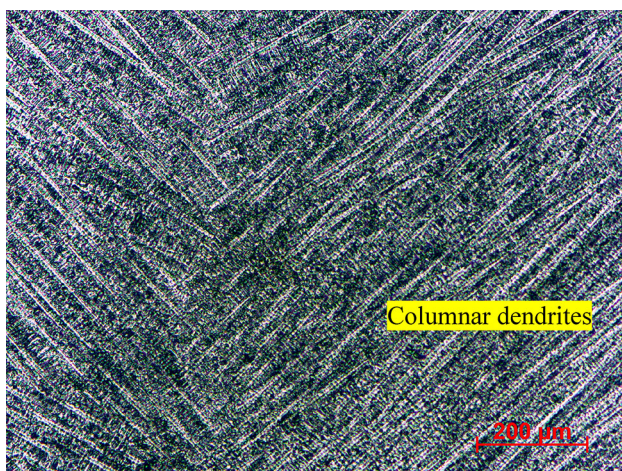


Figure 3. Weld centre microstructure of weld joint fabricated by EBW after aging treatment at 480°C for 3 h in air-cooled condition.

Hence, it can confirm that there is severe microsegregation of alloying elements in the weld center interdendritic region of weldments subjected to DA.

3.3 Solution-treated microstructure

Figure 5 shows a solution-treated microstructure of the weldment fabricated by EBW and it consists of columnar dendrites.

Post-weld ST at 980°C resulted in the dissolution of TCP phases to some extent but did not completely eliminate it. The temperature and soaking time required were not sufficient to cause significant microstructural change in this case. P phase occurs in the temperature range of 950–1050°C. Hence, it did not undergo any dissolution. However, the remaining two phases (σ and μ) were partially dissolved. Further, dissolution of secondary TCP phase purely depends on its size, morphology and solute (Mo and Cr) concentration. Figures 6(a) and (b) show higher magnification SEM micrograph of solution-treated EBW sample.

The micrograph shows the continuous secondary phase network in the form of long-chain interconnected particles observed in the interdendritic regions. As compared with the as-welded and aging-treated sample, the volume of secondary phases is more in the solution-treated sample. Figures 6 (i) and (ii) present the EDS results of solution-treated EBW sample in weld centre dendrite core and interdendritic region, respectively. SEM and EDAX analysis (figure 6 and table 5) also show coarse columnar structure by its existence and dense distribution of secondary TCP phases viewed as a continuous network.

Coarser, interconnected TCP phases at solute concentration need higher temperatures and longer soaking period for dissolution [24]. ST also causes the precipitation of Mo and Cr elements around the partially dissolved TCP phases to some extent but does not completely eliminate them. It occurs during weld metal solidification; the interdendritic regions become enriched with a high concentration of Mo and Cr, which results in continuous TCP phase network. Further, interdendritic segregation has not been evened out in the welds. Finally, ST heat treatment results in partial recrystallization and refinement of grains between matrix and TCP phases. This leads to augmentation in grain boundary strength and notch sensitivity at high temperature [14].

3.4 HT microstructure

Figure 7 shows the microstructure of alloy 686 after EBW, homogenization at 1200°C for 1 h and air cooling. The secondary phases in the weldment are dissolved into the austenite matrix, and complete recrystallization and

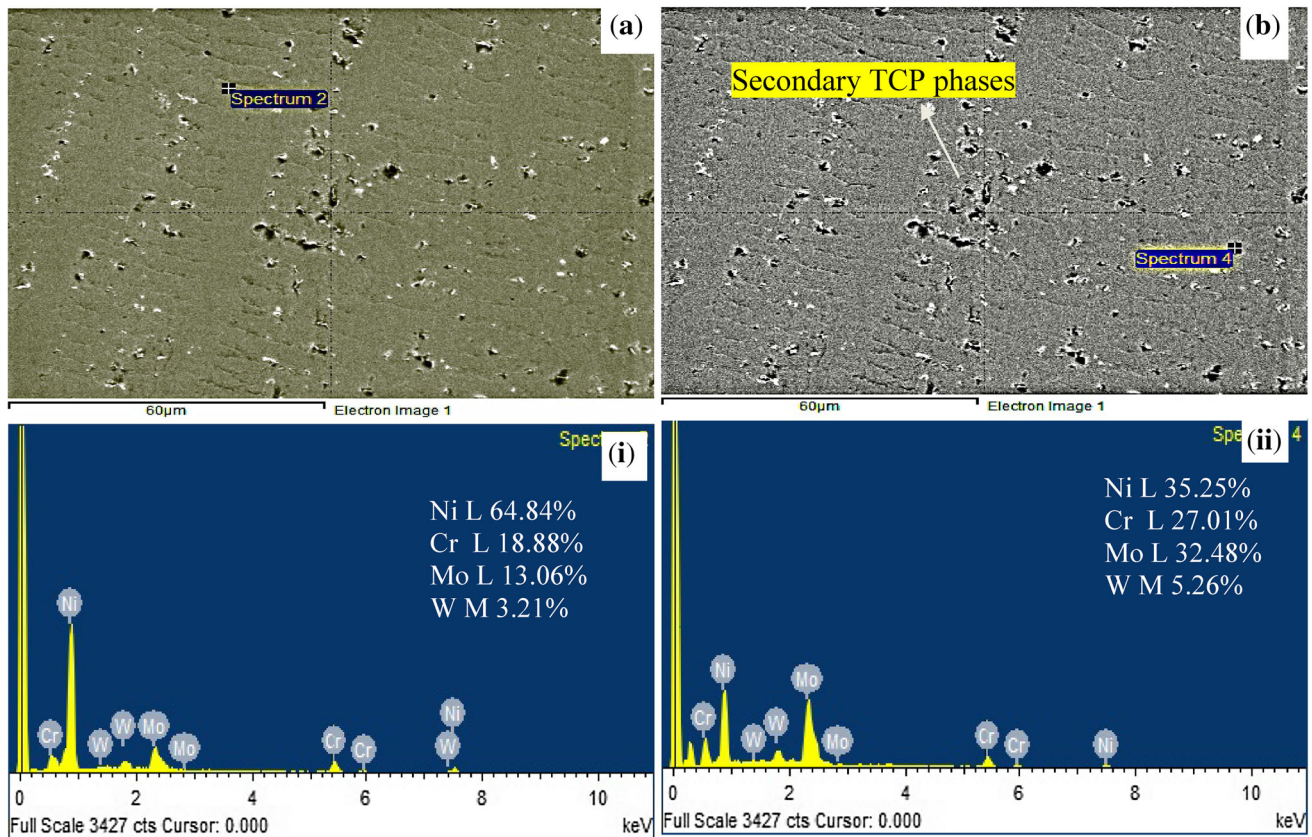


Figure 4. SEM/EDS analysis of aging and EBW weld Centre SEM image of (a) dendritic core, (b) interdendritic region, EDS analysis of (i) Weld Centre interdendritic region, (ii) weld centre dendritic core.

Table 4. EDS analysis of aged sample – elemental levels of the different zones after EBW of alloy 686.

Sl. no.	Zone	Ni	Cr	Mo	W
1	Dendritic core	64.84	18.88	13.06	3.21
2	Interdendritic region	35.25	27.01	32.48	5.26

significant microstructural change is observed in this condition and is entirely different from previous two cases. Since this treatment is carried out beyond TCP phases dissolving temperature, secondary phases (P , σ and μ phases) associated with alloy 686 are dissolved in the austenite matrix and uniformly distributed all over the matrix.

As can be seen, at 1200°C, the original dendritic structure has completely broken up and produced clear grain boundaries in the weld fusion zone. Complete recrystallization and grain growth were observed with clear grain boundaries. SEM images (figures 8(a) and (b)) present the presence of a minor amount of partially dissolved TCP phases. EDS analysis figures 8 (i) and (ii) and table 6 also confirm the slight Mo microsegregation of alloying elements in the interdendritic region. The interdendritic region is slightly enriched with Mo and W, and impoverished with Ni content. When compared with DA

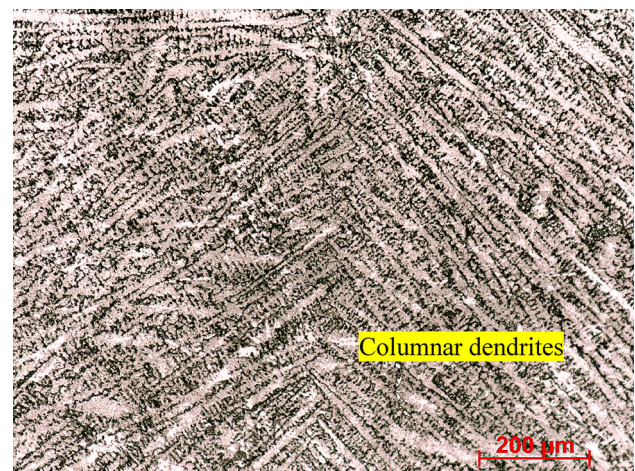


Figure 5. Weld center Microstructure of weld joint fabricated by EBW after solution treatment at 980 C/ air cooled + ST.

and ST cases, here the microsegregation is considerably less.

HT diminished the severity of interdendritic Mo segregation in the welds compared with the as-weld condition as a result of diffusion of Mo atoms into the dendrite core regions. A similar observation is noticed in Inconel 718 PWHT [25].

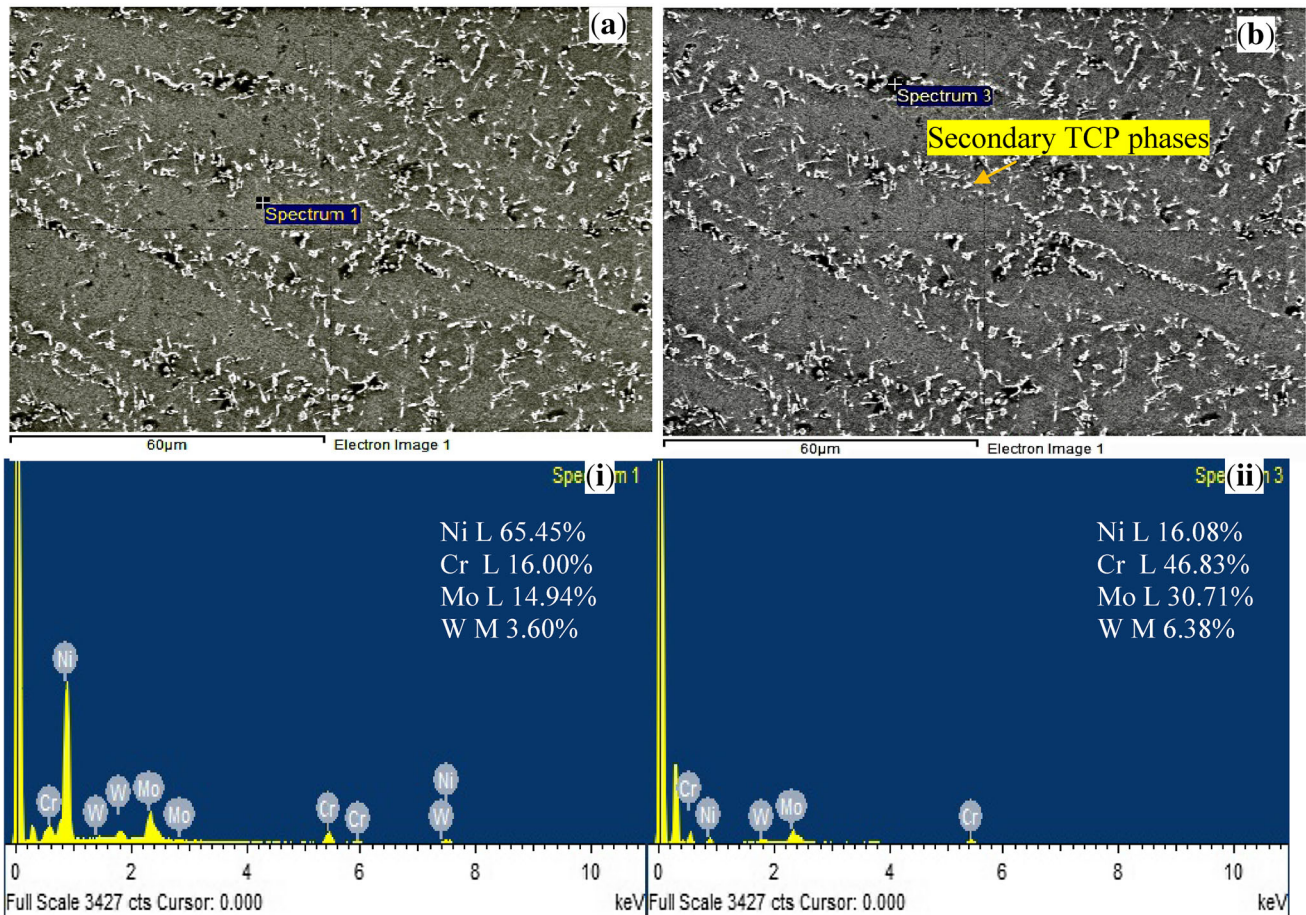


Figure 6. SEM/EDS analysis of Solution treated EB Weldment Weld Centre SEM image for (a) dendritic core, (b) interdendritic region, EDS analysis of (i) weld centre dendritic core, (ii) Weld Centre interdendritic region.

Table 5. EDS analysis of aged + solutionized sample – elemental levels of the different zones after EBW of alloy 686.

Sl. no.	Zone	Ni	Cr	Mo	W
1	Dendritic core	65.45	16.00	14.94	3.60
2	Interdendritic region	16.08	46.83	30.71	6.38

3.5 Tensile test

Table 7 shows the tensile test result obtained from the as-welded and different post-weld-heat-treated specimens. The results show that (i) EBW UTS is nearly matched with base metal strength, (ii) DA result shows some improvement in weld tensile properties compared with those of base metal, (iii) highest UTS is observed in ST condition and (iv) tensile properties in homogenization condition are inferior to base material properties. Moreover, ductility is very less in the as-EBW, ST and DA conditions. The ductility is the highest in homogenized condition, and tensile failure occurs in the base metal. Weld zone failure is noticed in as-EBW, ST and DA conditions.

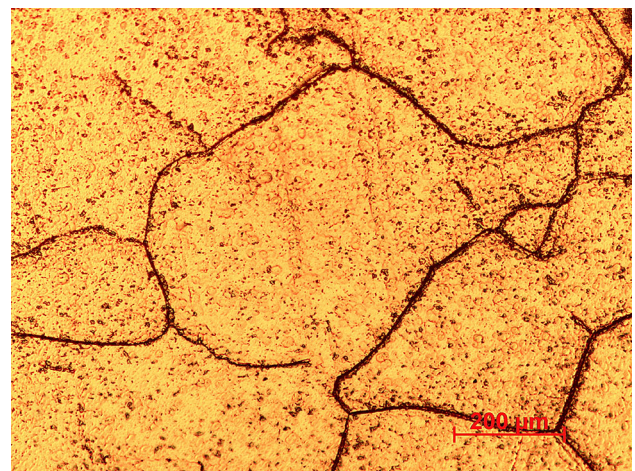


Figure 7. Weld centre microstructure of weld joint fabricated by EBW after homogenization at 1200°C/air cooling + DA+ST.

The tensile strength of alloy 686 after EBW and DA treatment is higher (981 MPa) than that of as-EBW and lower than that of solution-treated condition as shown in

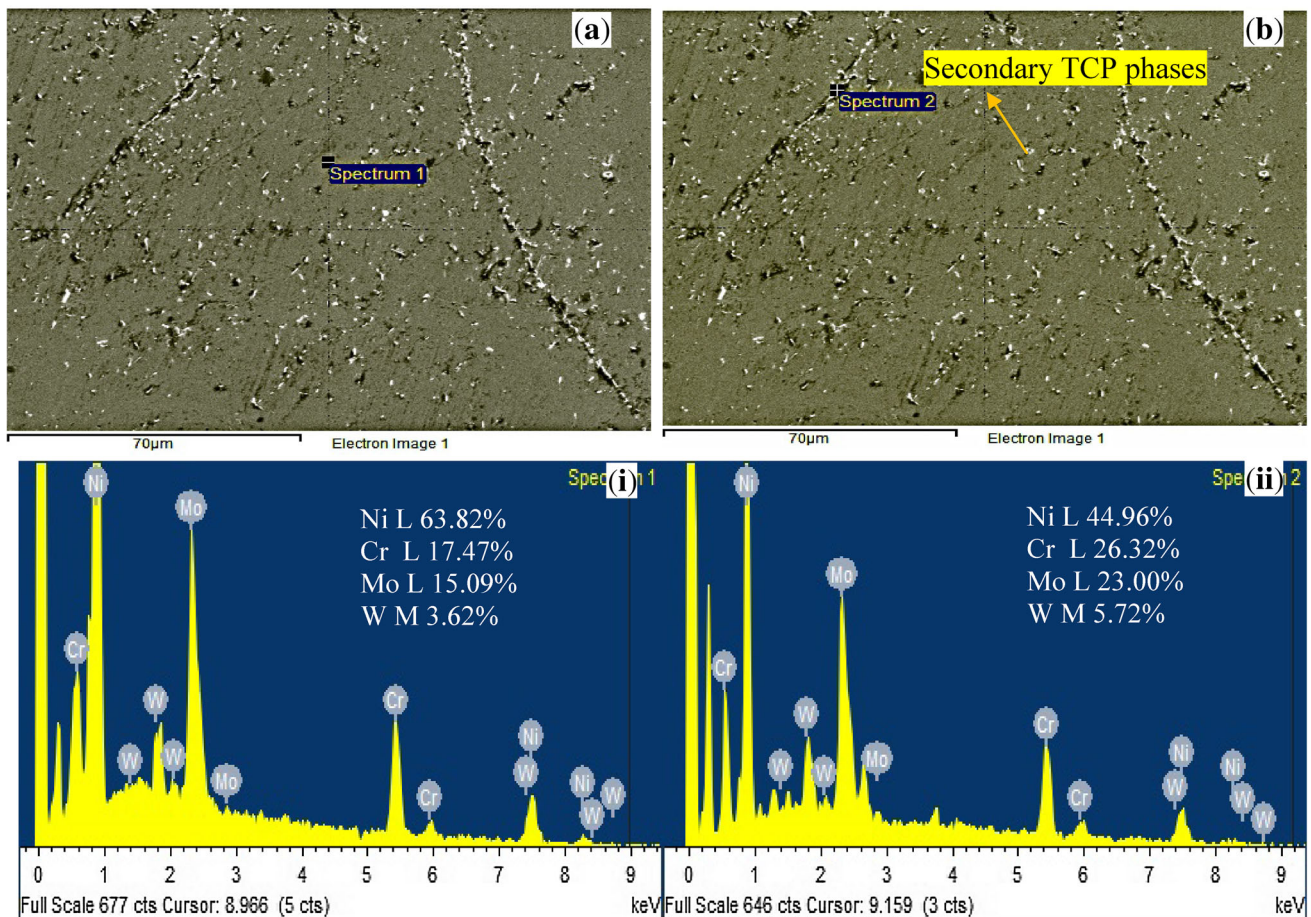


Figure 8. SEM/EDS Analysis of Homogenized EB weldment's Weld Centre: SEM image of (a) dendritic core, (b) interdendritic region, EDS analysis of (i) weld centre dendritic core, (ii) Weld Centre interdendritic region.

Table 6. EDS analysis of aged + solutionized + homogenized sample – elemental levels of the different zones after EBW of alloy 686.

Sl. no.	Zone	Ni	Cr	Mo	W
1	Dendritic core	63.82	17.47	15.09	3.62
2	Interdendritic region	50.22	30.34	16.37	3.08

Table 7. Tensile properties of the alloy 686 weldments at different heat treatment conditions.

Material condition	UTS (MPa)	Elongation (%)	Failure location
Base metal	813	61	–
As-electron-beam welded	815	21	Weld
Aging	981	21.513	Weld
Aging + solutionizing	1017	14.844	Weld
Aging + solutionizing + homogenizing	760	78.102	Base metal

table 7. The tensile failure took place at fusion zone weld centre. Secondary TCP phases offer strain effect against crack propagation, and it increases tensile strength moderately; on the other hand, it decreases the ductility.

The partial recrystallization during ST resulted in the improved tensile strength of weldment significantly to 1017 MPa, which is higher than that of other two counterparts. Re-distribution of alloying elements along grain boundary increases the solid strengthening effect, which results in the highest tensile strength. Continuous TCP phase's network and high solute concentration of alloying elements restrict the ductility to the lowest value among others.

The tensile strength of as-EBW alloy 686 is about 815 MPa, and it is decreased to 760 MPa in homogenized condition. The tensile strength of weld joint is associated with brittle secondary phases, alloying element's solid solution strengthening effect and residual stress [14]. Homogenization results in large size recrystallized grains which are larger than those of base metal FCC austenitic structure. It will result in a reduction of tensile strength and improved ductility.

4. Conclusions

In this research work, the effects of PWHT on the microstructure characteristics and tensile properties of Inconel 686 after EBW were studied. The results from this research study are summarized as follows:

1. The microstructure of as-EBW samples contains fine equiaxed dendrites at CFZ of weld centre whereas columnar dendrites are observed in transition fusion zone (TFZ) of weld centre. SEM/EDS results confirm the existence of secondary TCP phases.
2. No obvious change in microstructure was observed between as-EBW and DA-EBW samples. Since the aging temperature is much lower than secondary topologically closed packed (TCP) phases dissolving temperature, microsegregation is observed in the interdendritic region.
3. Partial recrystallization and refinement between the matrix and TCP phases were observed in ST microstructure. This results in enhanced notch sensitivity and grain boundary strength at high temperature.
4. Most of all secondary TCP phases (σ , P and μ) were dissolved into austenite matrix, completely recrystallized large grains were observed in HT microstructure and intensity of microsegregation was lower than in previous two cases.
5. The partial recrystallization and re-distribution of alloying elements during ST increase the solid solution strengthening effect, which results in significant improvement in tensile strength (1017 MPa), which is greater than the other two counterparts.

References

- [1] *Special metal data sheet*. <http://www.specialmetalswiggins.co.uk/pdfs/products/INCONEL%20alloy%20686.pdf> (accessed 08 August 2016)
- [2] Shoemaker L E and Crum J R 2015 Experience in effective application of metallic materials for construction of FGD systems. Spec. Met. Tech. data Sheet. http://pccforgedproducts.com/web/user_content/files/wyman/Metallic%20Materials%20for%20Construction%20of%20FGD%20Systems.pdf (accessed 08 August 2016)
- [3] Special metal data sheet: alloy 686. <http://www.specialmetals.de/files/INCONEL%20alloy%20686.pdf> (accessed 08 August 2016)
- [4] Shoemaker L E and Crum J R 2016 Nickel–chromium–molybdenum superalloys: the solution to corrosion problems in wet limestone FGD air pollution control systems. http://www.pccforgedproducts.com/web/user_content/files/wyman/Ni%20Cr%20Mo%20Alloys%20-%20Solution%20to%20Corrosion%20problems%20in%20Wet%20Limestone%20FGD%20Air%20Pollution%20Control%20Systems.pdf (accessed 08 August 2016)
- [5] Crum J R and Shoemaker L E 2015 Special alloys and overmatching welding products solve FGD corrosion problems. Special Metals Technical Data Sheet. <http://216.71.103.52/documents/Special%20Alloys%20and%20Overmatched%20Welding%20Products%20Solve%20FGD%20Corrosion%20Problems.pdf> (accessed 10 September 2016)
- [6] John Dupont N, John Lippold C and Samuel Kiser D 1999 *Welding Metallurgy and Weldability of Nickel-Base Alloys*. New Jersey: Wiley, pp. 47–98
- [7] Cao X, Rivaux B, Jahazi M, Cuddy J and Birur A 2009 Effect of pre- and post-weld heat treatment on metallurgical and tensile properties of Inconel 718 alloy butt joints welded using 4 kW Nd: YAG laser. *J. Mater. Sci.* 44: 4557–4571
- [8] Silva C C, Conrado Afonso R M, Ramirez A J, Motta M F, Miranda H C and Farias J P 2016 Assessment of microstructure of alloy Inconel 686 dissimilar weld claddings. *J Alloys Compd.* 684: 628–642
- [9] Manikandan M, Arivazhagan N, Nageswara Rao M and Reddy G M 2015 Improvement of microstructure and mechanical behavior of gas tungsten arc weldments of alloy c-276 by current pulsing. *Acta Metall. Sin.* 28(2): 208–215
- [10] Arulmurugan B and Manikandan M 2017 Development of welding technology for improving the metallurgical and mechanical properties of 21st century nickel based superalloy 686. *Mater Sci. Eng A* A69: 126–140
- [11] Arulmurugan B and Manikandan M 2018 Investigations on microstructure and corrosion behavior of superalloy 686 weldments by electrochemical corrosion technique. *IOP Conf. Ser. Mater. Sci.* 310(1): 012071
- [12] Arulmurugan B, Agilan M, Jerome S, Arivarasu M, Manikandan M, Srikanth A and Arivazhagan N 2018 Investigation of metallurgical and mechanical properties of 21st century nickel-based superalloy 686 by electron beam welding technique. *Sadhana Acad. Proc. Eng. Sci.* 43: 117. <https://doi.org/10.1007/s12046-018-0850-x>
- [13] Peasura P and Poopat B 2015 Investigation into the influence of post-weld heat treatment on the microstructure and hardness of Inconel X-750. *Adv. Mech. Eng.* 7(4): 1–11. <https://doi.org/10.1177/1687814015578396>
- [14] Zhang Y, Yang L, Chen T, Zhang W, Huang X and Dai J 2017 Investigation on the optimized heat treatment procedure for laser fabricated IN718 alloy. *Opt. LASER Technol.* 97: 172–179
- [15] Hong J K, Park J H, Park N K, Eom I S, Kim M B and Kang C Y 2008 Microstructures and mechanical properties of Inconel 718 welds by CO₂ laser welding. *J. Mater. Process. Technol.* 201: 515–520
- [16] Cortial F, Corrieu J M and Vernot-Loier C 1995 Influence of heat treatments on microstructure, mechanical properties, and corrosion resistance of weld alloy 625. *Metall. Mater. Trans. A* 26A: 1273–1286
- [17] Xing X, Di X and Wang B 2014 The effect of post-weld heat treatment temperature on the microstructure of Inconel 625 deposited metal. *J. Alloys Compd.* 593: 110–116
- [18] Madhusudhan Reddy G, Srinivasa Murthy C V, Srinivasa Rao K and Prasad Rao K 2009 Improvement of mechanical properties of Inconel 718 electron beam welds—influence of welding techniques and postweld heat treatment. *Int. J. Adv. Manuf. Technol.* 43: 671–680
- [19] Yu K, Jiang Z, Leng B, Li C, Chen S, Tao W, Zhou X and Li Z 2016 Effects of post-weld heat treatment on microstructure

- and mechanical properties of laser welds in GH3535 superalloy. *Opt. LASER Technol.* 81: 18–25
- [20] El-Dasher B S, Edgumbe T S and Torres S G 2006 The effect of solution annealing on the microstructural behavior of alloy 22 welds. *Metall. Mater. Trans. A* 37A: 1027–1038
- [21] Edgumbe Summers T S, Rebak R B and Seeley R 2000 Influence of thermal aging on the mechanical and corrosion properties of c-22 alloy welds. In: *Proceedings of the Minerals–Metals–Materials Society Conference*, St. Louis, MO, October 8–12, pp. 1–12
- [22] Rae C M F, Karunaratne M S A, Small C J, Broomfield R W, Jones C N and Reed R C 2000 Topologically close packed phases in an experimental rhenium-containing single crystal superalloy. In: *Proceedings of Superalloys 2000*, TMS – The Minerals, Metals and Materials Society, pp. 767–777
- [23] Belan J 2016 GCP and TCP phases presented in nickel-base superalloys. *Mater. Today Proc.* 3: 936–941
- [24] Janaki Ram G D, Venugopal Reddy A, Prasad Rao K and Madhusudhan Reddy G 2004 Control of Laves phase in Inconel 718 GTA welds with current pulsing. *Sci. Technol. Weld. Join.* 9(5): 390–398
- [25] Janaki Ram G D, Venugopal Reddy A, Prasad Rao K, Madhusudhan Reddy G and Sarin Sundar J K 2005 Microstructure and tensile properties of Inconel 718 pulsed Nd–YAG laser welds. *J Mater. Process. Technol.* 167: 73–82